Chinese Chemical Letters 35 (2024) 108313

Contents lists available at ScienceDirect

Chinese Chemical Letters

journal homepage: www.elsevier.com/locate/cclet

Dynamic cooperations between lattice oxygen and oxygen vacancies for photocatalytic ethane dehydrogenation by a self-restoring $LaVO_4$ catalyst

Fen Wei[1], Weichao Xue[1], Zhiyang Yu, Xue Feng Lu, Sibo Wang*, Wei Lin*, Xinchen Wang*

State Key Laboratory of Photocatalysis on Energy and Environment, College of Chemistry, Fuzhou University, Fuzhou 350108, China

ARTICLE INFO

Article history:
Received 31 January 2023
Revised 5 March 2023
Accepted 7 March 2023
Available online 11 March 2023

Keywords:
Photocatalysis
Ethane dehydrogenation
Ethene
$LaVO_4$
Oxygen vacancy

ABSTRACT

Thermocatalytic nonoxidative ethane dehydrogenation (EDH) is a promising strategy for ethene production but suffers from intense energy consumption and poor catalyst durability; exploring technology that permits efficient EDH by solar energy remains a giant challenge. Herein, we present that an oxygen vacancy (O_v)-rich $LaVO_4$ ($LaVO_4$-O_v) catalyst is highly active and stable for photocatalytic EDH, through a dynamic lattice oxygen ($O_{latt.}$) and O_v co-mediated mechanism. Irradiated by simulated sunlight at mild conditions, $LaVO_4$-O_v effectively dehydrogenates undiluted ethane to produce C_2H_4 and CO with a conversion of 2.3%. By loading a small amount of Pt cocatalyst, the evolution and selectivity of C_2H_4 are enhanced to 275 μmol h^{-1} g^{-1} and 96.8%. Of note, $LaVO_4$-O_v appears nearly no carbon deposition after the reaction. The isotope tracked reactions reveal that the consumed $O_{latt.}$ recuperates by exposing the used catalyst with O_2, thus establishing a dynamic cycle of $O_{latt.}$ and achieving a facile catalyst regeneration to preserve its intrinsic activity. The refreshed $LaVO_4$-O_v exhibits superior reusability and delivers a turnover number of about 305. The O_v promotes photo absorption, boosts ethane adsorption/activation, and accelerates charge separation/transfer, thus improving the photocatalytic efficiency. The possible photocatalytic EDH mechanism is proposed, considering the key intermediates predicted by density functional theory (DFT) and monitored by in-situ diffuse reflectance infrared Fourier transform spectroscopy (DRIFTS).

Ethene is a valuable platform chemical in modern chemical industry. The traditional route for ethene production is steam cracking of the naphtha from crude oil [1]. Alternatively, high-temperature cracking of ethane is another ethene production approach, because of the exploitation of shale gas that supplies abundant ethane over the past decade [2–4]. Although being used industrially, operating these two recipes requires harsh conditions, including high reaction temperature (>900 °C), coupled with fast outlet gas cooling (<800 °C) and short contact time (~0.3 s) to avoid overoxidation of ethene [5–7]. Apart from steam cracking, thermocatalytic oxidative and non-oxidative ethane dehydrogenation (EDH) to produce ethene have stimulated great interest in recent years [8–10]. The oxidative EDH involving an oxidant (*e.g.*, O_2) is thermodynamically favorable owing to the exothermic feature but suffers easily from overoxidation to form CO_2 [11,12]. Comparatively, the nonoxidative EDH bears an obvious merit in preventing overoxidation, yet this route usually encounters severe catalyst deactivation caused by coke formation and metal sintering at high temperatures [13], which imposes complex and even high-cost processes to regenerate the catalysts [14].

Besides thermal strategies, the technology of light-driven photocatalysis has recently exhibited immense vitality in dehydrogenation of alkanes to olefins [15–24], which enables the break of thermodynamic limitation and the handling of the reactions under mild conditions. For example, Pt^+-loaded black TiO_2 presents excellent conversion and high stability for cyclohexane dehydrogenation, but a much slower conversion rate for EDH, even at a very negative partial pressure [19]. Another photocatalytic EDH is achieved over Cu/TiO_2 under UV light irradiation, affording moderate conversion (1.7%) and high ethene selectivity (98.41%) using diluted ethane (10%) [20]. Despite these achievements, the study of photocatalytic EDH is just in its infancy, and it is challenging to realize efficient and selective light-initiated EDH for making ethene, especially those mediated by non-noble-metal catalysts in undiluted ethane.

Herein, we demonstrate the facile preparation of an O_v-rich $LaVO_4$-O_v photocatalyst, which displays high activity and stability

* Corresponding authors.
E-mail addresses: sibowang@fzu.edu.cn (S. Wang), wlin@fzu.edu.cn (W. Lin), xcwang@fzu.edu.cn (X. Wang).
[1] These authors contributed equally to this work.

https://doi.org/10.1016/j.cclet.2023.108313
1001-8417/

for EDH *via* dynamic collaborations between $O_{latt.}$ and O_v. The $LaVO_4$-O_v material is created through a one-pot hydrothermal method and characterized by diverse physiochemical techniques. Under simulated sunlight irradiation, pristine $LaVO_4$-O_v actively dehydrogenates pure C_2H_6 to form C_2H_4 (15.4 μmol h^{-1} g^{-1}) and CO (26.8 μmol h^{-1} g^{-1}) with a conversion of 2.3%. By depositing a small amount of Pt as a cocatalyst, the yield and selectivity of C_2H_4 are promoted to 275 μmol h^{-1} g^{-1} and 96.8%. Noteworthily, the photocatalyst appears nearly no coke formation after the reaction. The ^{13}C and ^{18}O labeled isotope reactions validate that C_2H_4 produces from C_2H_6, while CO originates from C_2H_6 and $O_{latt.}$. Importantly, the consumed $O_{latt.}$ can recover readily by contacting the catalyst with O_2 in air, which thus constructs a dynamic cycle of $O_{latt.}$ and achieves a simplistic catalyst regeneration. The restored $LaVO_4$-O_v displays good reusability and affords a turnover number of about 305 based on the determined catalytic-active sites. The O_v is revealed to strengthen optical harvesting, boost ethane capture/activation, and facilitate separation and migration of charge carriers, contributing to the augmentation of photocatalytic efficiency. DFT and *in-situ* DRIFTS identify the key intermediates in the EDH process and support the construction of the possible reaction mechanism.

The $LaVO_4$-O_v and $LaVO_4$ samples exhibit similar X-ray diffraction (XRD) patterns with all diffraction peaks indexed to a monoclinic $LaVO_4$ phase (Fig. 1a) [25]. The Fourier transform infrared spectra (FTIR) indicate that O_v formation affects the chemical feature of the VO_4^{3-} unit (Fig. S1 in Supporting information) [26,27]. The XPS survey spectra show only La, V and O elements, except C, indicating their high purities, and further analysis on La and V elements reveals the forms of La^{3+} and V^{4+}/V^{5+} cations (Fig. S2 in Supporting information) [27,28]. The asymmetric O 1s spectrum comprises three peaks with the dominant one at 529.7 eV (Fig. 1b), attributing to $O_{latt.}$. The additional two peaks at 530.5 and 532.0 eV correspond to O_v and surface adsorbed oxygen species ($O_{ads.}$), respectively [29–31]. Compared with $LaVO_4$-O_v, the V 2p and O 1s spectra of $LaVO_4$ are negatively shifted by about 0.2 eV, meaning that introducing O_v into $LaVO_4$ endows these elements with enriched electrons [32].

The defective structure of $LaVO_4$-O_v was probed by electron paramagnetic resonance (EPR). A strong signal (g = 1.977) is detected for $LaVO_4$-O_v, but not for $LaVO_4$ (Fig. 1c), which confirms the existence of O_v-related V^{4+} species [28]. Mesopores are revealed present in $LaVO_4$-O_v and $LaVO_4$ (Fig. S3 in Supporting information), and the former holds a larger specific surface area than the latter, which underlines that formation of O_v endows $LaVO_4$ with beneficial texture properties for heterogeneous photocatalysis.

The UV–vis diffuse reflectance spectra (DRS) indicate $LaVO_4$-O_v and $LaVO_4$ have broad light absorption in UV-visible region (Fig. 1d). Besides, $LaVO_4$-O_v exhibits a reinforced infrared harvesting, compared with $LaVO_4$, due to the presence of O_v that elevates the Fermi level and builds defect level in the bandgap [29,33-36]. The Tauc plots determine the bandgap energies (E_g) of $LaVO_4$-O_v (2.21 eV) and $LaVO_4$ (2.28 eV) (Fig. S4 in Supporting information). From the Mott-Schottky curves with positive slopes (Fig. S5 in Supporting information), the flat band potentials of $LaVO_4$-O_v and $LaVO_4$ are estimated at 0.46 and 0.50 V (*vs.* NHE), which are considered as their conduction band (CB) potentials. Therefore, the band structures of $LaVO_4$-O_v and $LaVO_4$ are defined (Fig. S6 in Supporting information).

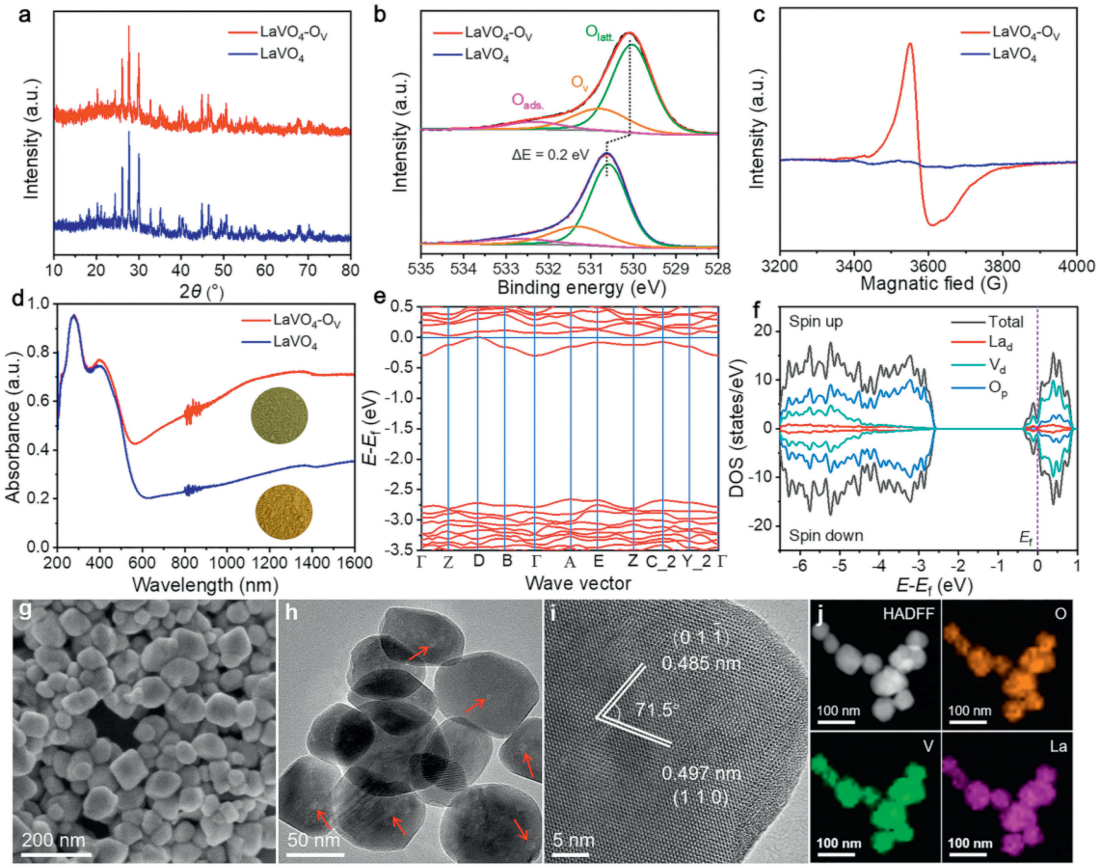

Fig. 1. (a) XRD patterns, (b) O 1s spectra, (c) EPR spectra, (d) DRS and colors of $LaVO_4$-O_v and $LaVO_4$. (e) The calculated band structure, (f) DOS, (g) FESEM image, (h) TEM image, (i) HRTEM image, and (j) EDS maps of $LaVO_4$-O_v.

The band structures and density of states (DOS) of $LaVO_4$-O_v and $LaVO_4$ were theoretically simulated. The modeled $LaVO_4$-O_v and $LaVO_4$ feature indirect bandgap with E_g values of about 2.4 and 2.5 eV (Fig. 1e and Fig. S7a in Supporting information), respectively, close to the experimental data. The DOS indicate that the Fermi levels of $LaVO_4$-O_v and $LaVO_4$ are located above the valence band (VB) maximum (Fig. 1f and Fig. S7b in Supporting information), due to perfect or lower energy electron filling. Moreover, the VBs are dominated by oxygen p-orbital, inferring that the photo-formed holes will retention on oxygen atoms for oxidation reactions, while the CBs consist of the d-orbitals of V and La with a localized electronic density of states. These results suggest that O_v not only shifts the Fermi level of $LaVO_4$, but also makes it overlap with the CB. Moreover, the small difference in the E_g values of $LaVO_4$-O_v and $LaVO_4$ reflects that the intensified photoabsorption of $LaVO_4$-O_v should be induced by oxygen defects on the surface, rather than in the bulk.

The field emission scanning electron microscopy (FESEM) image of $LaVO_4$-O_v presents a morphology of nanoparticles in size around 100 nm (Fig. 1g). The transmission electron microscopy (TEM) image exposes the presence of mesopores (indicated by arrows, Fig. 1h), which might be the result of ammonia gas release during the crystallization process. In the high-resolution TEM (HRTEM) image (Fig. 1i), two lattice spacing values of 0.485 and 0.497 nm, with an inclination angle of 71.5°, are well resolved, correspond to the $(01\bar{1})$ and (110) facets of monoclinic $LaVO_4$. Further analysis of the HRTEM image reveals that the particle has high crystallinity and dominantly exposes (110) facets on the surface [37]. Energy dispersive spectrometry (EDS) maps display the uniform distribution of La, V and O elements of the $LaVO_4$-O_v material (Fig. 1j).

Photocatalytic EDH activities of the samples were evaluated by simulated sunlight in pure ethane with a partial pressure of 1 atm, which are much harsh conditions compared with previous works using diluted ethane at negative pressures [19,20,38]. The $LaVO_4$ catalyst is active to the EDH reaction with C_2H_4 and CO as the main products (Fig. 2a). In comparison, $LaVO_4$-O_v presents a enhanced activity, affording C_2H_4 and CO at rates of 15.4 and 26.8 μmol h^{-1} g^{-1}, respectively, which corresponds to a C_2H_4 selectivity of 47.8% and a C_2H_6 conversion of 2.3%. The moderate C_2H_4 selectivity may result from the strong oxidizing ability of the photoinduced holes that leads to C_2H_4 overoxidation to form CO. However, the EDH efficiency is expected to be controllable by tailoring the active sites and redox potentials of $LaVO_4$-O_v. Positively, the preliminary results reveal that the yield rate and selectivity of C_2H_4 are improved to 275 μmol h^{-1} g^{-1} and 96.8% by depositing Pt as a cocatalyst (Fig. 2b), and detailed studies are ongoing in our group. The high performance of $LaVO_4$-O_v is mainly attributed to the presence of Ov, serving as active sites for the EDH reaction. Also, O_v enhances light-to-heat conversion to drive the reaction. Specifically, $LaVO_4$-O_v with a strong infrared absorption delivers a higher photo-to-thermal conversion than $LaVO_4$ (Fig. S8 in Supporting information), that is, 170 °C for $LaVO_4$-O_v and 130 °C for $LaVO_4$.

Interestingly, CO produces from EDH without an oxidant, indicating CO should come from C_2H_6 oxidation by $O_{latt.}$ of the catalysts. The participation of $O_{latt.}$ is mirrored by the time-dependent activity of $LaVO_4$-O_V, showing a gradual decay in the 4 h reaction (the first cycle, Fig. 2c), due to consumption of catalytic-active O_{latt} and formation excessive O_v. To assess the reusability, the used $LaVO_4$-O_v is employed to catalyze two sets of 4h-reaction, but appears substantial deactivation (Fig. S9 in Supporting information). In another test, when the used $LaVO_4$-O_v is first exposed to air for regeneration and then re-applied to run the reaction repeatedly, it well preserves the original activity (Fig. 2c). These highlight that $O_{latt.}$ realizes regeneration by exposure to air, attaining a dynamic cycle of $O_{latt.}$ and the recovery of its intrinsic activity [21,39,40], together with its color becomes almost the same to the fresh sample (Fig. S10 in Supporting information). In other words, $LaVO_4$-O_v holds an oxygen storage/release ability, like the well-studied CeO_2 [41,42]. Therefore, CeO_2 is also utilized for photocatalytic EDH, but just exhibits negligible activity (Fig. 2a), which however stresses the superior performance of $LaVO_4$-O_v.

Control experiments indicate no product yields without $LaVO_4$-O_v, C_2H_6, or photoirradiation (Fig. S11 in Supporting information), suggesting that excitation of the photocatalyst triggers the EDH

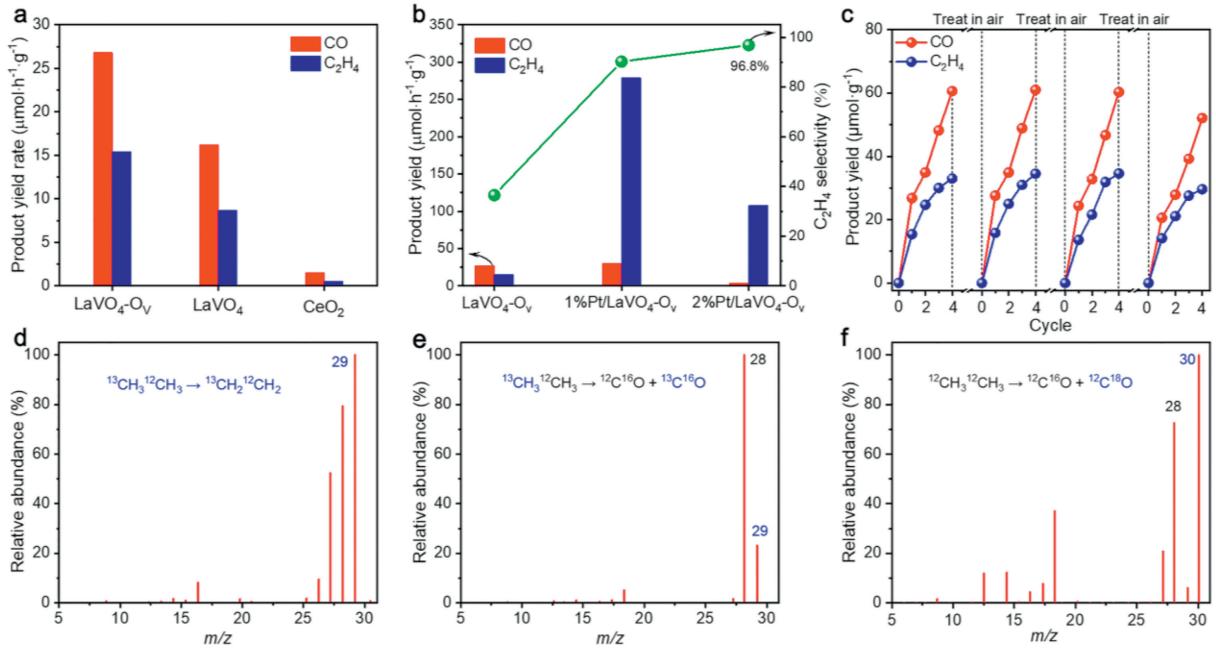

Fig. 2. (a) Photocatalytic ODE performance of different samples, (b) activities of $LaVO_4$-O_v and Pt/$LaVO_4$-O_v samples, (c) activity cycling tests of $LaVO_4$-O_v after regeneration. MS spectra of (d) C_2H_4 and (e) CO produced from the $^{13}CH_3{}^{12}CH_3$ isotope experiment, and (f) CO produced from $^{12}CH_3{}^{12}CH_3$ over the used $LaVO_4$-O_v after regenerating with $^{18}O_2$.

reaction. To estimate the contribution of thermal-catalysis, EDH is conducted at 200 °C (higher than 170 °C in photocatalysis) in dark, just affording a small C_2H_4/CO production (Fig. S11), emphasizing the high EDH efficiency stems primarily from photocatalysis.

XRD, XPS and TEM reveal no crystal, surface, and structural changes for $LaVO_4$-O_v after activity cycling tests (Fig. S12 in Supporting information), highlighting the outstanding stability of the photocatalyst after regeneration. Moreover, thermogravimetry (TG) and TG-mass spectroscopy (TG-MS) tests disclose nearly no noticeable carbon deposition forms on spent $LaVO_4$-O_v (Fig. S13 in Supporting information), which underlines the superiority of photocatalysis in preventing coke formation.

^{13}C and ^{18}O labeled isotope experiments were conducted to track the origin of C_2H_4 and CO. First, the fresh $LaVO_4$-O_v is employed for dehydrogenating $^{13}CH_3{}^{12}CH_3$. The MS spectrum of C_2H_4 gives dominated fragments of $^{13}CH_2{}^{12}CH_2$ ($m/z = 29$) (Fig. 2d and Fig. S14 in Supporting information), while those of CO are indexed to ^{13}CO ($m/z = 29$) and ^{12}CO ($m/z = 28$) (Fig. 2e). Such results confirm that C_2H_4 derives from C_2H_6, while CO comes from C_2H_6 and $O_{latt.}$. In the ^{18}O-labeled experiment, the used $LaVO_4$-O_v is exposed to $^{18}O_2$ for regeneration, and then applied to catalyze $^{12}CH_3{}^{12}CH_3$ conversion, which results in the detections of main $C^{18}O$ ($m/z = 30$) and $C^{16}O$ ($m/z = 28$) (Fig. 2f), proving $O_{latt.}$ recovery of the catalyst from molecular O_2 [43]. Such isotope experiments solidly validate the sources of C_2H_4 and CO and directly illustrate the dynamic $O_{latt.}$ loop of $LaVO_4$-O_v.

The steady-state photoluminescence (PL) and time-resolved PL (TR-PL) spectra reveal that $LaVO_4$-O_v manifests inhibited recombination and promoted separation of light-induced carriers, compared with $LaVO_4$ (Fig. S15 in Supporting information). Meanwhile, the electrochemical impedance spectra (EIS) indicate $LaVO_4$-O_v retains a lowered charge-transfer resistance than $LaVO_4$ (Fig. S16a in Supporting information), and the transient photocurrent responses reflect electron transfer in $LaVO_4$-O_v is much faster than that in $LaVO_4$ (Fig. S16b in Supporting information). These findings suggest O_v formation promotes separation and migration of the charges, thus boosting photocatalytic EDH efficiency.

Temperature-programmed desorption of ethane (C_2H_6-TPD) was carried out to probe the active sites of $LaVO_4$-O_v and $LaVO_4$. The C_2H_6-TPD profiles exhibit two broad signals centered at around 250 and 500 °C (Fig. 3a), attributing to physical and chemical adsorption of ethane, respectively. The corresponding peak areas of $LaVO_4$-O_v are greater than that of $LaVO_4$, indicating O_v of $LaVO_4$-O_v promotes ethane adsorption. The determined number of active sites on $LaVO_4$-O_v is about 2.68 μmol/g, and hence, the turnover number of the catalyst in the activity cycling tests reaches 305, confirming the catalytic nature of the photo-driven EDH reaction.

The redox abilities of the catalysts were estimated by temperature-programmed reduction of hydrogen (H_2-TPR) and O_2-TPD. The H_2-TPR profiles of $LaVO_4$-O_v and $LaVO_4$ display two peaks at around 485 and 650 °C (Fig. 3b), relating respectively to reduction of surface adsorbed oxygen and $O_{latt.}$ [44]. Besides, the reduction peaks of $LaVO_4$-O_v appear at the lower temperatures, indicative of its enhanced oxidation ability. Three desorption peaks are observed in the O_2-TPD profile of $LaVO_4$-O_v (Fig. 3c). The strongest desorption below 300 °C links to surface adsorbed oxygen species ($O_{ads.}$) [44]. The small peak at around 330 °C is ascribed to the desorption of surface lattice oxygen ($O_{s\text{-}latt.}$), which is reactive and affects catalytic properties [45]. The desorption above 350 °C represents the release of bulk lattice oxygen ($O_{b\text{-}latt.}$) [44,46], reflecting the structural stability. Compared to $LaVO_4$-O_v, $LaVO_4$ exhibits a markedly diminished desorption of $O_{sorb.}$, owing to its absence of O_v that reduces surface O_2 adsorption. Furthermore, no clear desorption of $O_{s\text{-}latt.}$ evolves for $LaVO_4$ because the lack of O_v makes

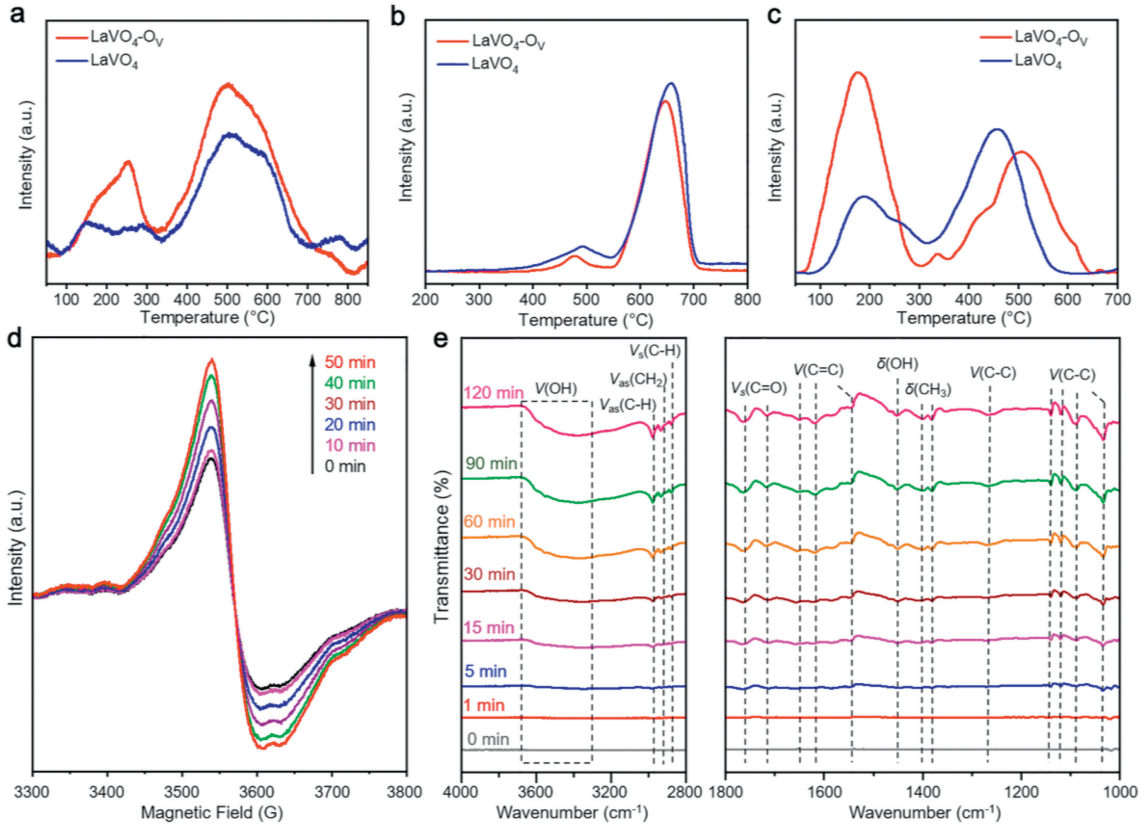

Fig. 3. (a) C_2H_6-TPD, (b) H_2-TPR and (c) O_2-TPD profiles of $LaVO_4$-O_v and $LaVO_4$. (d) *In situ* EPR spectra of $LaVO_4$-O_v in C_2H_6 under varied conditions. (e) *In situ* DRIFTS spectra of $LaVO_4$-O_v in C_2H_6 under light irradiation for different durations.

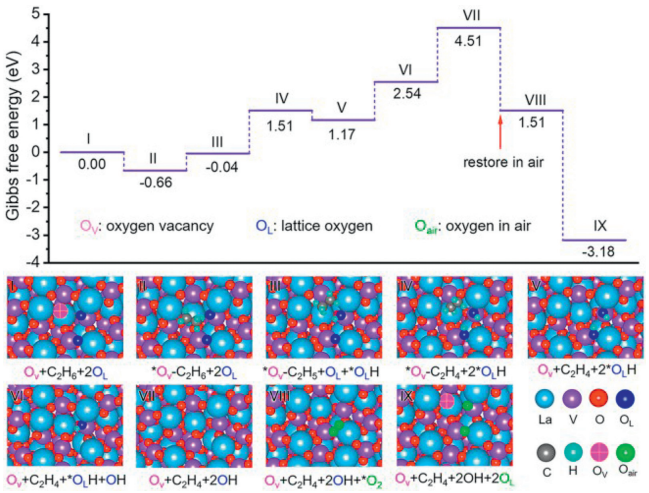

Fig. 4. Calculated potential energy diagram and the corresponding optimized geometries of active species over $LaVO_4$-O_v by DFT.

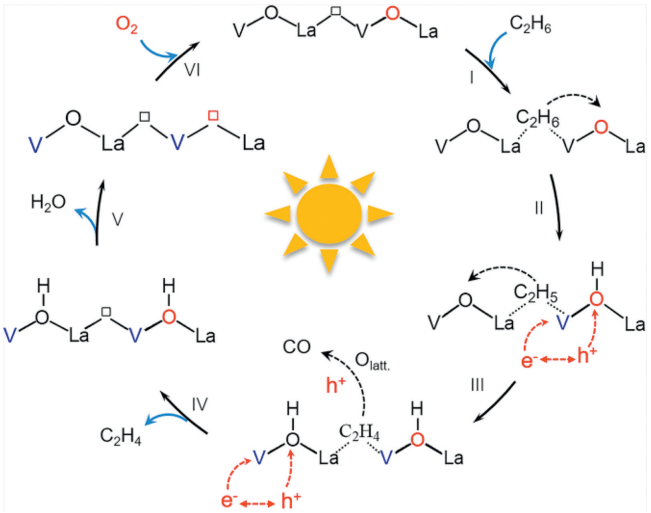

Fig. 5. The proposed photocatalytic EDH mechanism over $LaVO_4$-O_v (the black box represents the O_v of fresh $LaVO_4$-O_v, and the red box represents the O_v created from the consumption of $O_{latt.}$ during the reaction).

its $O_{s\text{-}latt.}$ more stable. In addition, the desorption of $O_{b\text{-}latt.}$ of $LaVO_4$ presents at a lower temperature, revealing the higher structural stability of $LaVO_4$-O_v. These results confirm $LaVO_4$-O_v possess high redox ability, rich active sites, and enhanced oxygen storage capability.

To probe the reactive oxygen species and structural changes of the $LaVO_4$-O_v photocatalyst, *in situ* EPR measurements were conducted. The EPR signal assigned to O_v-related V^{4+} species intensifies regularly according to the prolongation of irradiation time (Fig. 3d), which signifies the enrichment of O_v, due to the release of $O_{latt.}$ for running the EDH reaction.

In-situ DRIFTS was employed to identify intermediates and elucidate processes of EDH. After adsorbing C_2H_6 in dark, $LaVO_4$-O_v exhibits five distinct peaks assigned to stretching vibrations of C–H bonds (Fig. S17 in Supporting information) [17,20], suggesting efficient C_2H_6 adsorption by the catalyst. Upon light irradiation, signals of several new species are detected with the intensities heightened by prolonging the photoirradiation (Fig. 3e). The gradually enhanced band at 3680–3058 cm^{-1} reflects the accumulation of H_2O (Table S1 in Supporting information) [47,48]. The vibrations of C–H (2975 and 2875 cm^{-1}) and CH_2 (2930 cm^{-1}) bonds imply the generation of the key intermediates of CH_3–CH_2· and ·CH_2–CH_2· [17,20,49], which may be generated from dissociation adsorption of C_2H_6 on O_v. The involvements of these key species are also supported by detected vibrations corresponding to CH_3 (1400 and 1380 cm^{-1}) and C-C (1265, 1138, 1118, 1089 and 1031 cm^{-1}) moieties. Notably, observation of featured vibrations of C=O (1763 and 1716 cm^{-1}) and C=C (1650, 1619 and 1545 cm^{-1}) bonds reveals the formation of CO and C_2H_4 [50–52]. In addition, the vibration at 1452 cm^{-1} points to the evolution of OH species during the reaction [17,48].

Based on the results of photocatalytic EDH, we further performed DFT calculations to explore the thermodynamic favorability of C_2H_6 transformation and $O_{latt.}$ consumption. The reaction mechanism of alkane dehydrogenation co-steered by O_v and $O_{latt.}$ has not been thoroughly tracked and deciphered on $LaVO_4$-O_v. This mysterious mechanism is expected to be decoded on the recyclable $LaVO_4$ benchmark platform. The $LaVO_4$-O_v catalyst allows O_v to capture C_2H_6 with a low adsorption energy of −0.66 eV (Fig. 4, from I to II). The adjoining lattice oxygens are responsible for subsequent bonding with H to generate OH (Fig. 4, from III to IV). The upward trend in free energy until complete desorption of 2OH (Fig. 4, from V to VII), discloses that ethane dehydrogenation to ethene is a challenging process that requires photothermal energy to drive. After that, it is very favorable for the adsorption of O_2 because of a downward trend in energy (Fig. 4, VIII), which can perfectly refill the consumed $O_{latt.}$ sites after decomposing into two oxygen atoms (Fig. 4, IX). Such theoretical results are in good agreement with the hao de activity cycling tests. In contrast, $LaVO_4$ without O_v is inferior in both ethane adsorption and OH desorption (Fig. S18 in Supporting information), demonstrating the effectiveness of more stable intrinsic O_v in EDH, rather than metastable O_v generated by depleting $O_{latt.}$.

The photocatalytic EDH process is proposed based on the experimental and theoretical results (Fig. 5). Initially, C_2H_6 is preferentially adsorbed on O_v of $LaVO_4$-O_v (step I). Upon light irradiation, the photoinduced holes are trapped by surface $O_{latt.}$ to produce active $O^{\bullet-}$ species [21], which enables H abstraction from adsorbed C_2H_6, yielding the C_2H_5/C_2H_4 fractions and adsorbed OH groups (steps II and III). Concurrently, the electrons reduce V^{5+} to form V^{4+}, which is supported by XPS analyses on used $LaVO_4$-O_v catalyst (Fig. S19a in Supporting information). Afterward, the C_2H_4 species release from catalyst surface to generate ethene gas (step IV), while the adsorbed OH groups desorb in form of H_2O (step V), rendering the catalyst with decreased $O_{latt.}$ and increased O_v (Fig. S19b in Supporting information). Due to the strong oxidative ability of photogenerated holes, overoxidation of C_2H_4 also occurs in cooperation of $O_{latt.}$, resulting in CO release. Lastly, being exposed to O_2, V^{4+} cation reduces O_2 to $O_{latt.}$ positioned in the lattice with itself oxidized to V^{5+} (step VI), achieving a dynamic cycle of $O_{latt.}$ and catalyst regeneration, which finishes the catalytic loop.

In summary, demonstrated herein is the facile synthesis of a $LaVO_4$-O_v catalyst with O_v and its function in light-driven EDH under mild conditions. The photocatalytic EDH reaction follows a mechanism mediated dynamically by $O_{latt.}$ and O_v. Bare $LaVO_4$-O_v grants effective dehydrogenation of undiluted C_2H_6 to produce C_2H_4, together with CO, while Pt-loaded $LaVO_4$-O_v affords greatly enhanced C_2H_4 production and selectivity. Remarkably, $LaVO_4$-O_v shows an excellent coking-resistant property and achieves fine reusability *via* a simplistic regeneration with air exposure to restore the depleted $O_{latt.}$; while its O_v promotes optical absorption, ethane adsorption/activation, and charge separation/transport to boost the photocatalytic efficiency. This work may advance the feasibility of photocatalysis technology for EDH with renewable solar resource. Also, the recoverable catalytic-active $O_{latt.}$ of $LaVO_4$-O_v is anticipated to extend for driving some oxidant-sensitive organic transformations in a heterogeneous fashion.

Declaration of competing interest

The authors declare that they have no known competing financial interests or personal relationships that could have appeared to influence the work reported in this paper.

Acknowledgments

This work is financially supported by the National Key R&D Program of China (Nos. 2021YFA1502100 and 2022YFE0114800) and the National Natural Science Foundation of China (No. 21973014).

Supplementary materials

Supplementary material associated with this article can be found, in the online version, at doi:10.1016/j.cclet.2023.108313.

References

[1] T. Amrillah, A.R. Supandi, V. Puspasari, A. Hermawan, Z.W. Seh, Trans. Tianjin Univ. 28 (2022) 307–322.
[2] J.M. Venegas, W.P. McDermott, I. Hermans, Acc. Chem. Res. 51 (2018) 2556–2564.
[3] R. Yao, J.E. Herrera, L. Chen, Y.H.C. Chin, ACS Catal. 10 (2020) 6952–6968.
[4] Y. Zhou, F. Wei, J. Lin, et al., ACS Catal. 10 (2020) 7619–7629.
[5] Z. Maeno, S. Yasumura, X. Wu, et al., J. Am. Chem. Soc. 142 (2020) 4820–4832.
[6] J. Liu, N. He, Z. Zhang, et al., ACS Catal. 11 (2021) 2819–2830.
[7] M. Numan, E. Eom, A. Li, et al., ACS Catal. 11 (2021) 9221–9232.
[8] J.J.H.B. Sattler, J. Ruiz-Martinez, E. Santillan-Jimenez, B.M. Weckhuysen, Chem. Rev. 114 (2014) 10613–10653.
[9] Y. Bian, M. Kim, T. Li, A. Asthagiri, J.F. Weaver, J. Am. Chem. Soc. 140 (2018) 2665–2672.
[10] S. Najari, S. Saeidi, P. Concepcion, et al., Chem. Soc. Rev. 50 (2021) 4564–4605.
[11] Y. Pan, A. Bhowmick, W. Wu, et al., ACS Catal. 11 (2021) 9970–9985.
[12] R. Jin, M. Peng, A. Li, et al., J. Am. Chem. Soc. 141 (2019) 18921–18925.
[13] M.D. Porosoff, M.N.Z. Myint, S. Kattel, et al., Angew. Chem. Int. Ed. 54 (2015) 15501–15505.
[14] Z. Yang, H. Li, H. Zhou, et al., J. Am. Chem. Soc. 142 (2020) 16429–16436.
[15] C. Zhao, M. Xi, J. Huo, C. He, L. Fu, Chin. Chem. Lett. 34 (2023) 107213.
[16] Q. Li, H. Yue, C. Liu, et al., Chem. Eng. J. 395 (2020) 125120.
[17] R. Zhang, H. Wang, S. Tang, et al., ACS Catal. 8 (2018) 9280–9286.
[18] Q.H. Zheng, C. Chen, S.M. Cao, et al., Chin. Chem. Lett. 34 (2023) 107273.
[19] L. Zhang, L. Liu, Z. Pan, et al., Nat. Energy 7 (2022) 1042–1051.
[20] L. Song, R. Zhang, C. Zhou, et al., Chem. Commun. 59 (2023) 478–481.
[21] S. Song, H. Song, L. Li, et al., Nat. Catal. 4 (2021) 1032–1042.
[22] S. Shoji, X. Peng, A. Yamaguchi, et al., Nat. Catal. 3 (2020) 148–153.
[23] D. Gao, W. Li, H. Wang, G. Wang, R. Cai, Trans. Tianjin Univ. 28 (2022) 245–264.
[24] L. Chen, Q. Liu, J. Yang, Y. Li, G. Li, Chin. Chem. Lett. 34 (2023) 107335.
[25] Y. Xu, J. Liu, M. Xie, et al., Chem. Eng. J. 357 (2019) 487–497.
[26] Y. He, J. Cai, L. Zhang, et al., Ind. Eng. Chem. Res. 53 (2014) 5905–5915.
[27] L. Jing, Y. Xu, J. Liu, et al., Appl. Catal. B 277 (2020) 119245.
[28] S. Wang, T. He, P. Chen, et al., Adv. Mater. 32 (2020) 2001385.
[29] S. Wang, B.Y. Guan, X.W. Lou, Energy Environ. Sci. 11 (2018) 306–310.
[30] F. Yang, X. Bao, P. Li, et al., Angew. Chem. Int. Ed. 58 (2019) 14179–14183.
[31] Y. Wang, C. Zhang, R. Li, Trans. Tianjin Univ. 28 (2022) 227–235.
[32] B. Zhang, Y. Chang, Y. Wu, et al., Adv. Energy Mater. 12 (2022) 2200321.
[33] W. Wei, Z. Wei, R. Li, et al., Nat. Commun. 13 (2022) 3199.
[34] W. Zhang, C. Fu, J. Low, et al., Nat. Commun. 13 (2022) 2806.
[35] W. Fan, H. Li, F. Zhao, et al., Chem. Commun. 52 (2016) 5316–5319.
[36] Y. Zhao, C. Chang, F. Teng, et al., Adv. Energy Mater. 7 (2017) 1700005.
[37] Y. Guo, B. Yan, F. Deng, et al., Chin. Chem. Lett. 34 (2023) 107468.
[38] L. Liu, H. Li, H. Zhou, et al., Chem 9 (2023) 637–649.
[39] X. Yu, V.L. Zholobenko, S. Moldovan, et al., Nat. Energy 5 (2020) 511–519.
[40] Y. Fang, Q. Zhang, H. Zhang, et al., Angew. Chem. Int. Ed. 61 (2022) e202212273.
[41] Y. Zhang, S. Zhao, J. Feng, et al., Chem 7 (2021) 2022–2059.
[42] N. Daelman, M. Capdevila-Cortada, N. López, Nat. Mater. 18 (2019) 1215–1221.
[43] J. Di, Y. Li, Y. Zhang, et al., Trans. Tianjin Univ. (2022), doi:10.1007/s12209-022-00344-9.
[44] S. Wu, H. Liu, Z. Huang, H. Xu, W. Shen, Appl. Catal. B 312 (2022) 121387.
[45] L. Zhang, Y. Liu, X. Fang, Y. Cheng, Fuel 321 (2022) 124116.
[46] Y. Wang, R. Liu, M. Shi, et al., Chin. Chem. Lett. 34 (2023) 107200.
[47] N. Li, B. Wang, Y. Si, et al., ACS Catal. 9 (2019) 5590–5602.
[48] W. Wang, C. Deng, S. Xie, et al., J. Am. Chem. Soc. 143 (2021) 2984–2993.
[49] L. Wang, B. Zhao, C. Wang, et al., J. Mater. Chem. A 8 (2020) 10175–10179.
[50] W. Jiang, J. Low, K. Mao, et al., J. Am. Chem. Soc. 143 (2021) 269–278.
[51] F. Tian, H. Zhang, S. Liu, et al., Appl. Catal. B 285 (2021) 119834.
[52] W. Gao, S. Li, H. He, et al., Nat. Commun. 12 (2021) 4747.